©2008 The Visualization Society of Japan
Journal of Visualization, Vol. 11, No. 1 (2008)37-44

Regular Paper

Flow Visualization and Aerodynamic-Force Measurement of a Dragonfly-Type Model

□im□ S. □.[1]□ C□ang□ □.[2] and So□n□ M. [3] □.□

*1 Department of Aerospace and Mechanical Engineering, Korea Aerospace University, Hwajeon-dong, Deokyang-gu, Goyang city, Gyeonggi-do, 412-791, Republic of Korea.
*2 Department of Aeronautical Science and Flight Operation, Korea Aerospace University, Hwajeon-dong, Deokyang-gu, Goyang city, Gyeonggi-do, 412-791, Republic of Korea. E-mail: jwchang@kau.ac.kr
*3 Department of Aerospace Engineering, Korea Air Force Academy, Ssangsuri, Namil-myun, Chungwon-gun, Chungbuk-do, 363-849, Republic of Korea.

Received 9 March 2007
Revised 19 September 2007

Abstract : An unsteady flow visualization and force measurement were carried out in order to investigate the effects of the reduced frequency of a dragonfly-type model. The flow visualization of the wing wake region was conducted by using a smoke-wire technique. An electronic device was mounted below the test section in order to find the exact position angle of the wing for the visualization. A load-cell was employed in measuring aerodynamic forces generated by a plunging motion of the experimental model. To find the period of the flapping motion in real time, trigger signals were also collected by passing laser beam signals through the gear hole. Experimental conditions were as follows: the incidence angles of the fore- and hind-wing were 0° and 10°, respectively, and the reduced frequencies were 0.150 and 0.225. The free-stream velocities of the flow visualization and force measurement were 1.0 and 1.6m/sec, respectively, which correspond to Reynolds numbers of 3.4×10^3 and 2.9×10^3. The variations of the flow patterns and phase-averaged lift and the thrust coefficients during one cycle of the wing motion were presented. Results showed that the reduced frequency was closely related to the flow pattern that determined flight efficiency, and the maximum lift coefficient and lift coefficient per unit of time increased with reduced frequency.

Keywords : Dragonfly-type Model, Flow visualization, Reduced frequency, Leading-edge vortex, Lift, Drag.

1. Introduction

In contrast to aircraft with fixed wings, birds and insects produce effective lift and thrust through a flapping motion. This flapping mechanism is composed of plunging and pitching motions. Fejtek and Nehera (1980) measured the aerodynamic force and moment of a plunging motion of a NACA8331 airfoil and concluded that maximum lift and thrust were produced during the middle of the downstroke wing motion. Dickinson and Gotz (1993) showed that the leading-edge vortex generated at the leading-edge and reattached at the trailing edge of flapping wings, and that a separation bubble developed between the leading and trailing edges. Willmott et al. (1997) explained that the separation bubble increased the effective camber, and this enhanced lift generation by the increase of local velocity on the wing's upper surface. Van den Berg and Ellington (1997) conducted a visualization study using a smoke-wire technique and showed that reattachment of the leading-edge vortex occurred during the downstroke motion. Further, Liu et al. (1998) numerically studied a hawk-moth's wing motion and showed that lift was generated during the downstroke phase of the motion. Lastly, Chang and Sohn (2006) performed a numerical study of the fling-clapping motion of a rigid flat-plate wing pair that might be employed by insects, and presented flow patterns and

aerodynamic force data.

Research on the flapping motion of a pair of wings has made substantial progress recently. However, there exist insufficient and controversial data on two-pair wings, like those of dragonfly. Alexander (1982) argued that a dragonfly flies with a phase difference of 90°, generally, but in some cases it uses phase differences of 180° or 0° (for example, if it needs a large instantaneous force). Previous studies on insects with two pairs of wings indicated that they are more efficient flyers than insects with only one pair of wings. Saharon and Luttges (1988) carried out a flow visualization study on dragonfly wings and showed that the flow pattern of the dragonfly wing has roughly eight distinct vortex structures depending on the wing's kinematics: pitching, plunging, and scrolling. Okamoto (1996) experimentally investigated the aerodynamics of dragonflies with main interest on the effect of wing shape, such as camber and thickness.

2. Experimental Set-Up and Procedure

In this study, flow visualization and aerodynamic force measurement were carried out for a dragonfly-type model that resembled a real dragonfly as closely as possible. The visualization and the aerodynamic force measurement were done with models of different size, but at the same reduced frequency in order to satisfy dynamic similarity. The model executed a heaving motion only because it had the limitation of the 4-bar plane linkage mechanism.

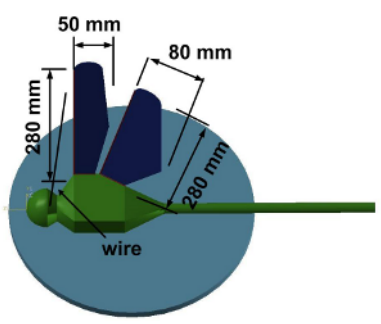

Fig. 1. Model for flow □isualization.

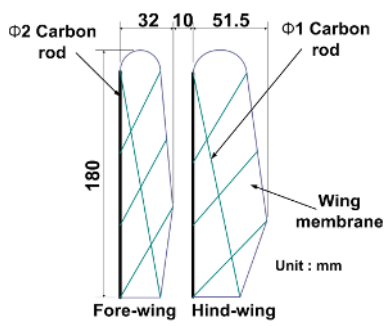

Fig. 2. □ing structure of t□e model for force measurement.

In the present study, a half model was tested by assuming the flow pattern of the dragonfly-type model with two pairs of wings is symmetrical. Figure 1 shows the half model used for flow visualization, which is dynamically similar to a real dragonfly. The fore-wing of the flow-visualization model has a wingspan of 280 mm and a mean chord length of 43 mm, and the hind-wing has a wingspan of 280 mm and a mean chord length of 59.8 mm. The wing of the force-measurements model is made of an aluminum metalized PET (Poly Ethylence Terephthalate) film (for wing surface) and carbon rods of diameter 2 mm and 1 mm (for the wing structure) as shown in Fig. 2. When the fore and hind wings were positioned at a wing position angle of 0°, the incidence angles of the fore and hind wings between the chord line and the free-stream velocity were 0° and 10°, respectively. The instantaneous wing position angle varied from -16.5° to +22.8°. The smoke-wire was installed perpendicular to the wing and the flow direction, and was located 2.51C (C: mean chord length of the hind-wing) from the wing tip of the fore-wing and 0.59C from the leading edge of the fore-wing. The range of the reduced frequency was determined based on Chasman and Chakravarthy (2001), who used a dragonfly model seven-times larger in size than a real dragonfly and chose

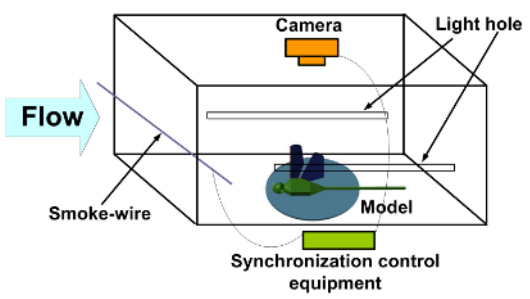

Fig. 3. Experimental set-up for flow □isualization.

Fig. 4. Model for force measurements.

wing beat frequencies of 0.57, 1.00 and 1.59, which match the beat frequencies of real dragonflies, in order to achieve dynamic similarity. The wing beat frequencies in the present study were determined as 0.96 and 1.43, which correspond to the reduced frequencies of K = 0.150 and 0.225, respectively.

Figure 3 shows the experimental device and model for flow visualization in the test section, which has a width of 0.5 m, height of 0.5 m, and length of 1.5 m. The free-stream velocity for flow visualization was fixed at 1.0 m/sec, which corresponds to the chord Reynolds number of 3.4×10^3. The streamwise view over the wings was recorded by the camera positioned on the roof of the test section, and synchronization control equipment linked to the camera was used to find the exact position angle of the wing (Corke et al., 1974). The synchronization control equipment in this experiment was also used in order to control the smoke generation and the photographic time. When the synchronization control circuit was connected to the variable position of the wing gear, the circuit applied power to the smoke-wire and the camera photographed flow patterns at 1.57 second intervals. Three frames of photographs per second were obtained with a Nikon F-100 camera loaded with ISO 400 film at an exposure time of 1/8,000 sec. Uncertainties in the wing position angles were estimated to be less than 1.0°.

Figures 4 and 5 show the dragonfly-type model in the test section used for the aerodynamic force measurements. The wind tunnel used is a close-circuit type, has a square test section of 1.0 m in both height and width, and can produce a maximum speed of 45.1 m/sec. For the force measurements, the free-stream velocity was fixed at 1.6 m/sec in order to obtain the same reduced frequency and wing beat frequency in the flow visualization. The Reynolds number in the force measurement experiment was 2.9×10^3 based on the free-stream velocity and the chord length of the model. The force measurement employed a 63 %-scaled model of the half one used in the visualization in order to reduce the wall interference effect. The plunging angle varied from -19.0° to 25.0° in order to have the similarity with the flow visualization experiment, and the fore- and hind-wing incidence angles were 0° and 10°, respectively.

Figure 6 shows a definition of the lift and drag for the dragonfly-type model. The resultant aerodynamic force can be resolved into two components: parallel and perpendicular to the free-stream. The hind-wings create the component of the force that is parallel to the free-stream due to the incidence angle of 10°.

Figure 7 shows the calibration curve of the load-cell used in the aerodynamic force measurement. In this figure, the X and Y axes show force (N: Newton) and voltage of the load-cell (V: voltage), respectively.

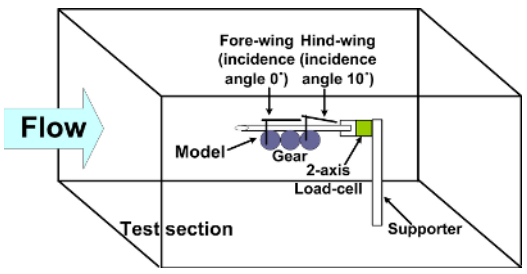

Fig. □. Experimental set-up for force measurements.

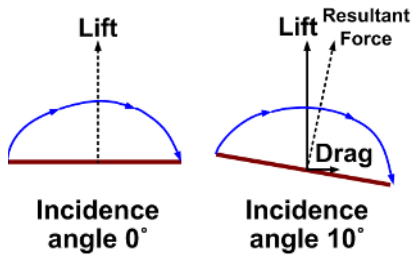

Fig. □. S□etc□ s□owing lift and drag.

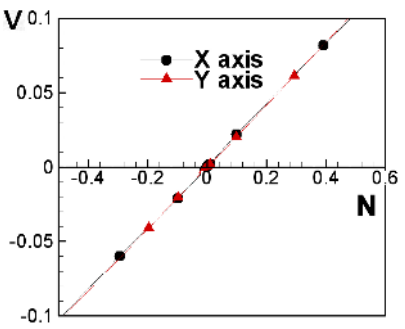

Fig. □. □oad-cell cali□ration.

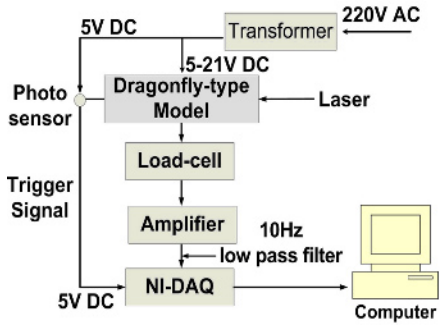

Fig. □. Data ac□uisition system.

Force interference errors of the load-cell along the X and Y axes were 0.58 % and 2.4 %, respectively. A flow chart diagram of the data acquisition system used in the force measurement is shown in Fig. 8. Aerodynamic force data, after passing through a 10 Hz low-pass filter and amplifier, was compiled to a computer. To find the period of the flapping motion in real time, trigger signals were collected by passing laser beam signals through the gear hole which were then received by a photo sensor on the other side and displayed at 5 V.

Figure 9 shows the force data measured in the wind-tunnel and vacuum-chamber during one cycle of the flapping motion. In this figure, the X and Y axes show force (N: Newton) and dimensionless time (t: physical time, T: time period of one cycle), respectively. The pure aerodynamic force data were obtained by subtracting the vacuum-chamber data from the wind-tunnel data. The experimental model was composed of gears, connecting-loads, and a motor so that the inertia force was included in the force data of the experimental model performing flapping motion in the test section of the wind tunnel. Singh et al. (2004) used a vacuum-chamber with a 90 % vacuum condition in order to eliminate the inertia force generated by the mechanical flapping model in the test section of the wind tunnel. In the present study an additional effort was made to get a real force data exempt from the inertia force of the experimental model. Figure 10 shows the vacuum chamber of the present study which can maintain a 99.99 % vacuum condition. The diameter of the vacuum chamber was 700 mm and the height was 860 mm. The effect of the number of data units on the ensemble average value of the force data was examined. In total, an ensemble average of 95 instantaneous data were produced, which was sufficient to yield a converged value.

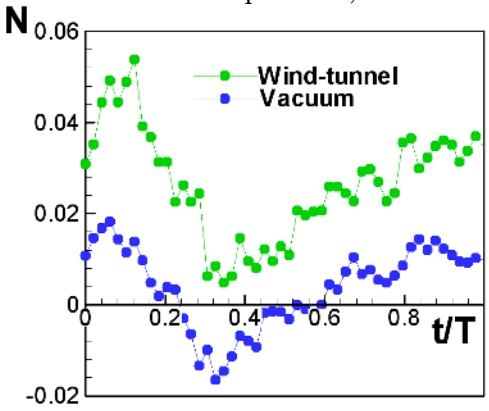

Fig. □. Typical wind-tunnel and vacuum chamber data.

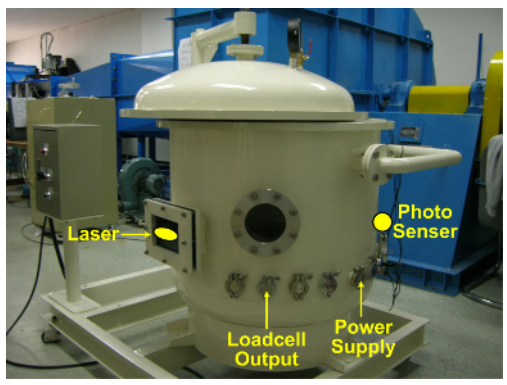

Fig. 1□. Vacuum chamber.

3. Result and Discussion

In the present study, both visualization and aerodynamic force measurements were performed in order to investigate the effects of the reduced frequency of a dragonfly-type model. Aerodynamic force data was compared to visualization pictures for the two reduced frequencies of K = 0.150 and 0.225. Figure 11 shows a streamwise view of the flow field near the wings at several instantaneous wing position angles. The phase difference of the fore-wing and the hind-wing was 90°. The subscribed numbers under each picture denote the wing position angles of the fore-wing and hind-wing, and the letters “u” and “d” represent upstroke and downstroke, respectively. Figure 12 shows the wing position angle and aerodynamic force data during one cycle of wing motion. Each motion phase of the flow visualization pictures in Fig. 11 is denoted on the motion and force histories in Fig. 12, in which a positive C_N value represents lift and thrust coefficient and a negative C_N value represents weight and drag coefficient.

The fore- and hind-wings shown in Fig. 11(a) are in a downstroke motion. Figure 11(a) shows that the leading-edge vortex (LEV) re-attached on the upper side of the fore-wing, but did not appear on the upper-side of the hind-wing, which was in an early stage of the downstroke motion as shown in the wing-position-angle history in Fig. 12(a). The fore- and hind-wings in Fig. 11(b) are also in the downstroke motion. The lift coefficient at the wing motion phase (b) was larger than that of the wing motion phase (a) as shown in Fig. 12 (b). Fejtek and Nehera (1980) showed that maximum lift and thrust were produced during the down-

stroke motion of the flapping wing. As shown in Fig. 12(a), the fore-wing of the wing motion phase (b) is at the end of the down-stroke motion, and the hind-wing is in the down-stroke motion and has a larger angular velocity than that of the wing motion phase (a). Therefore, the fore-wing generates less lift while the hind-wing generates more lift. The hind-wing of the dragonfly-type wing model in the present study was larger than the fore-wing, as is the case for a real dragonfly. It is thus argued that the large value of the lift coefficient during the wing motion phase (b), as shown in Fig. 12(b), was caused by the hind-wings of larger wing area, which was at the middle phase of the down-stroke wing motion.

Figure 12(b) shows that the experimental model in the present study had a positive lift coefficient of relatively large value in the wing motion phase (c) where the fore-wing was in the upstroke phase and the hind-wing was in the downstroke phase. An LEV (leading-edge vortex) was generated at the leading edge of the fore-wing and reattached to the trailing edge of the hind-wing, which contributed to making the flat wing of the dragonfly-type model into an airfoil shape and generating positive lift. At the wing motion phase (d), the LEV re-attached on the lower side of the fore-wing as shown in Fig. 11(d). Thus, the fore-wing had a lift coefficient of negative value, and the hind-wing had a lift coefficient of the smallest magnitude because it was in the end phase of the downstroke wing motion (Fejtek and Nehera, 1980). The lift coefficient increased slightly as the wing motion proceeded from phase (d) to phase (e), as shown in Fig. 12(b). The wing

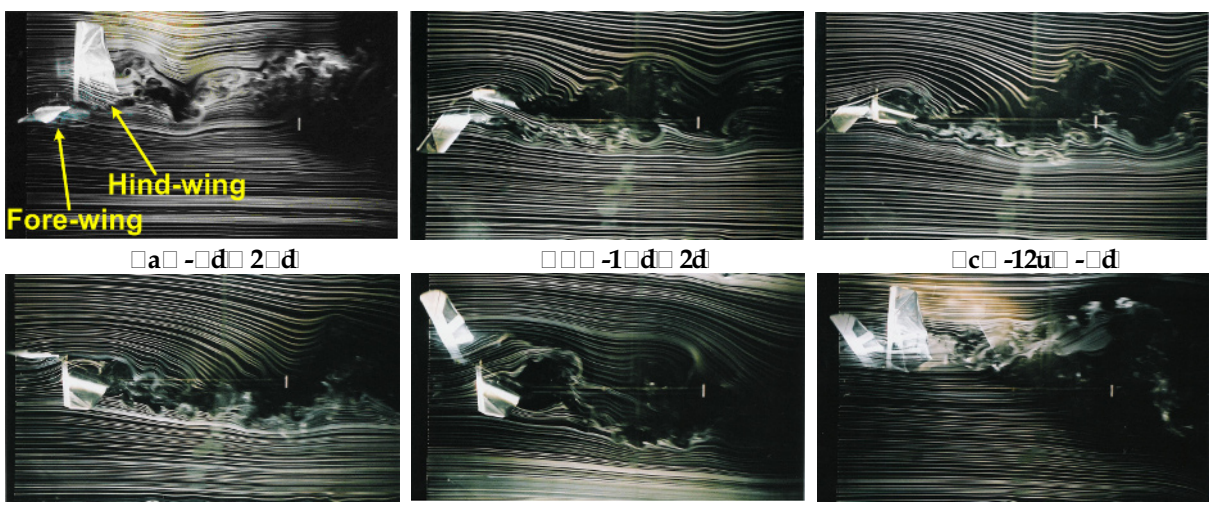

□a□ -□d□ 2□d□ □□□ -1□d□ 2d□ □c□ -12u□ -□d□

□d□ -□u□ -1□d□ □e□ 1□u□ -13u□ □f□ □d□ 21u□

Fig. 11. Flow □isualization of a dragonfly-type model at □ □ □.1□□.

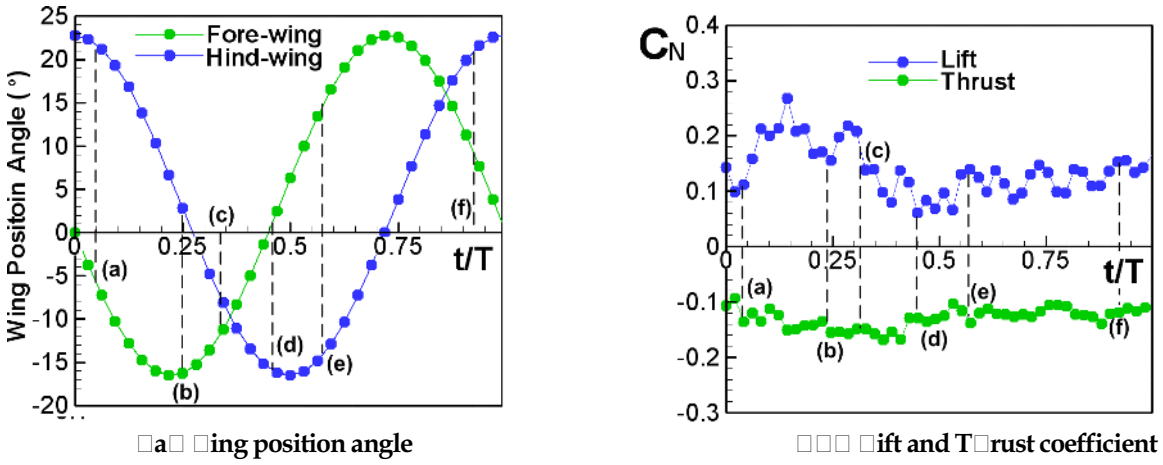

□a□ □ing position angle □□□ □ift and T□rust coefficient

Fig. 12. □ing position angle and aerodynamic c□aracteristics at □ □ □.1□□.

in the plunging phase with zero incidence angle generated lift slightly greater than the minimum lift generated at the middle phase of the upstroke. As shown in the flow visualization picture of Fig. 11(e), the fore-wing with zero incidence angle crossed the middle of the stroke where its angular velocity decreased. This made it difficult to find an LEV. However, the hind-wing at non-zero incidence angle started from the upstroke phase, which made an LEV to appear on the lower side of the hind-wing (not shown). Both the lift coefficient and the thrust coefficient changed a little during phases (e) and (f), as shown in Fig. 12(b). This was caused by the interaction between the lift increased by the fore-wing, which was in the middle phase of the fast downstroke motion, and the lift decreased by the hind-wing, which was in the end phase of the slow upstroke motion.

Thrust coefficient history during one cycle of the wing motion is shown in the lower graph of Fig. 12 (b). It was observed that the thrust coefficient changed a little during the whole wing motion phase. Fejtek and Nehera (1980) showed that the drag coefficient increased when the lift coefficient increased, and the drag coefficient decreased when the lift coefficient decreased for a flapping wing. The present study shows that re-attachment of the LEV is manifested in the wing motion phases of Figs. 11(b) and (c), where the lift vector is inclined to the free-stream by the non-zero incidence angle of the hind-wing. However, the lift generated by the re-attachment of the LEV on the fore-wing with zero incidence angle has no component in the free-stream direction. It can be said that the drag is mainly determined by the re-attachment structure of the LEV and the incidence angle of the wings. The results of Figs. 11 and 12 lead to the conclusion that the lift of the dragonfly-type wing increases during the down-stroke motion and is dominated by the motion of the hind-wing, which has the larger wing area.

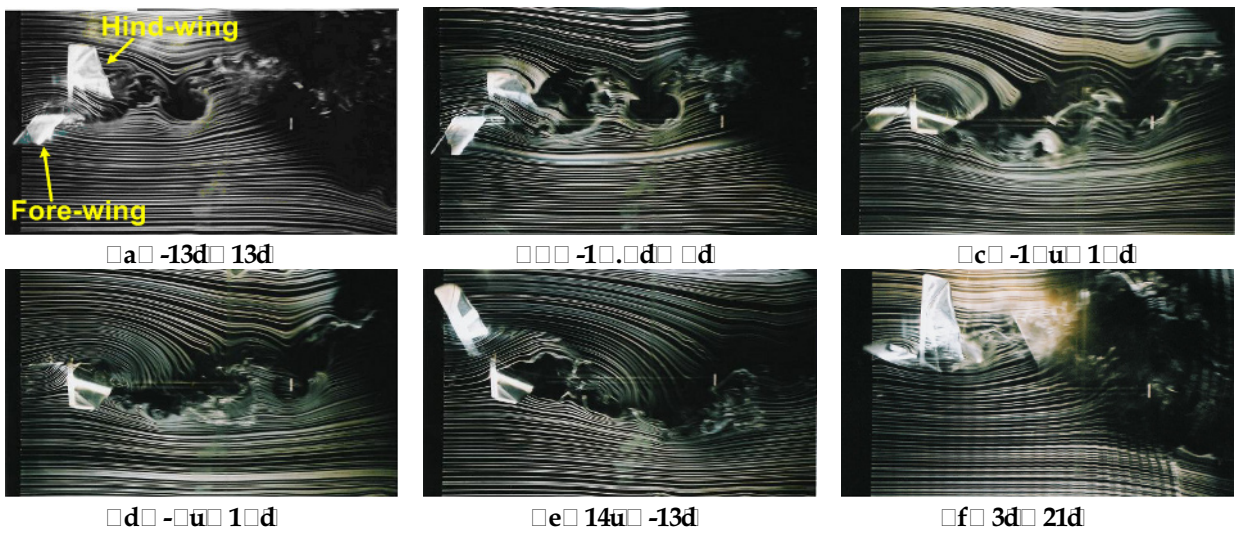

□a□ -13d□ 13d□□□ -1□.□d□ □d□c□ -1□u□ 1□d

□d□ -□u□ 1□d□e□ 14u□ -13d□f□ 3d□ 21d

Fig. 13. Flow □isualization of a dragonfly-type model at □ □ □.22□.

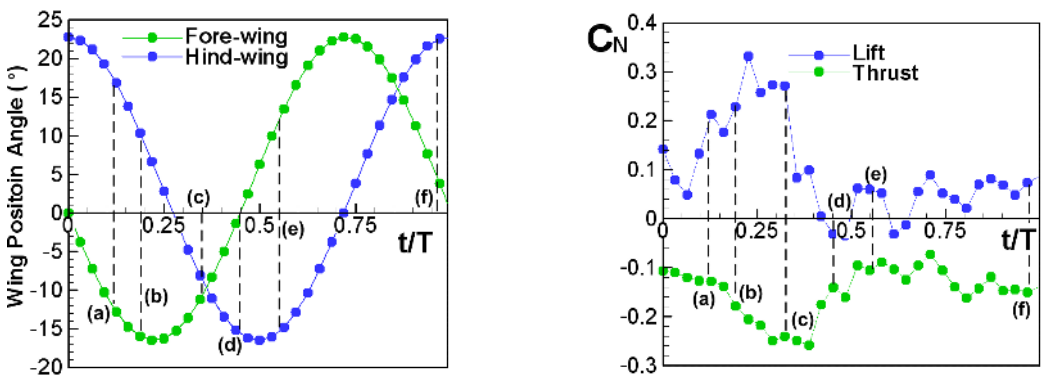

□a□ □ing position angle□□□ □ift and T□rust coefficient

Fig. 14. □ing position angle and aerodynamic c□aracteristics at □ □ □.22□.

Figure 13 shows the flow visualization results at the reduced frequency of K = 0.225 and a phase difference of 90°. Each frame of Fig. 13 is again denoted on the wing motion and force histories of Fig. 14. It is observed that that the streaklines around the wing in Fig. 13 are more curved than those in Fig. 11. The streaklines over the wing are curved downward and the streaklines under the wing are attached during the downstroke motion. The flow pattern around the wing model looks similar to that of a conventional airfoil in high-lift condition due to the LEV reattachment.

Figure 14 shows the wing position angles and the aerodynamic force coefficients during one cycle of wing motion. The aerodynamic characteristics in Fig. 14(b) show a similar tendency to that in Fig. 12(b). However, the value of the maximum lift coefficient of Fig. 14(b) where the reduced frequency was 0.225 is significantly different from that of Fig. 12(b) where the reduced frequency was 0.150. The streaklines of the larger curvature observed in Fig. 13 are thought to generate a larger value of the maximum lift coefficient at the reduced frequency of 0.225. The reduced frequency is a function of the free-stream velocity, the flapping frequency of the wing motion, and the wing chord-length. In the present study, only the plunging frequency of the wing motion was changed at the fixed free-stream velocity and chord length. The results of the present study showed that the streaklines with larger curvature reattached longer on the wing surface with increased flapping frequency. Either LEVs were generated on the leading edge and reattached on the trailing edge of the hind-wing, as shown in Fig. 13(c), or vortices were generated and reattached under the leading edge of the fore-wing, as shown in Fig. 13(d). The reattachment phenomena shown in Fig. 13 were observed to be more pronounced than those shown in Fig. 11. The flow phenomena observed in the visualization results validated the characteristics of the aerodynamic force data. The lift coefficient valve at the position (c) of Fig. 14(b) was 0.28 at the reduced frequency of 0.225, and that at the position (c) of Fig. 12(b) was 0.20 at the reduced frequency of 0.150. Thus the lift coefficient during one wing-motion cycle increased as the reduced frequency increased. The resultant aerodynamic force was inclined to the free-stream due to the incidence angle (10°) of the hind-wings. The large values of drag (negative thrust) shown in Fig. 14(b) are caused by the horizontal component of the resultant aerodynamic force generated by the hind-wing with incidence angle of 10°.

The mean values of the lift coefficients integrated during one cycle of the wing motion were 0.142 at K = 0.150 and 0.100 at K = 0.225. However, the value of the maximum lift coefficient at K = 0.225 was larger than that at K = 0.150. The lower value of the mean lift coefficient at K = 0.225 is due to the increase of the lift force of opposite sign. The results of the present study show that the mean values of lift coefficients in unit time were 0.142 at K = 0.150 and 0.150 at K = 0.225. The duration of the flapping period of the K = 0.225 case was smaller than that of the K = 0.150 case. Therefore, the lift coefficient per unit time increased as the reduced frequency increased. Thrust is shown in the lower graph of the aerodynamic force histories of Fig. 14(b). Total drag also increased at the higher reduced frequency due to the increased value of the lift generated by the hind-wings.

4. Conclusion

The present study investigated the effects of the reduced frequency of a dragonfly-type model with two pairs of wings at low Reynolds numbers. The fore-wing and hind-wing had a phase difference of 90°, and had incidence angles of 0° and 10°, respectively. The reduced frequencies of the wing motion tested were 0.150 and 0.225.

The streaklines on the upper surface of the model wing were attached to the wing surface while the streaklines on the lower surface of the model wing were bent in the upstroke direction during the upstroke wing motion. However, the streakline on the upper surface bent in the downstroke direction while the streakline on the lower surface attached to the wing surface during the downstroke wing motion. The curvature of the streaklines and the LEV re-attachment phenomena increased as the reduced frequency increased. The reattachment of LEV was mainly responsible for the lift generation. Both the value of the maximum lift coefficient and the lift coefficient per unit time increased as the reduced frequency of the wing motion increased. The larger values of drag were caused by the horizontal component of the resultant aerodynamic force in the hind-wing which had an incidence angle of 10°.

Acknowledgments

This work was supported by the Korea Research Foundation Grant. (KRF-2004-041-D00145)

References

Alexander, D. E., Studies on Flight Control and Aerodynamics in Dragonflies, (1982), Ph. D. Dissertation, Duke University, Durham, NC.
Chang, J. W. and Sohn, M. H., Numerical Flow Visualization of First Cycle and Cyclic Motion of a Rigid Fling-Clapping Wing, Journal of Visualization, 9-4 (2006), 381-391.
Chasman, D. and Chakravarthy, S., Computational and Experimental Studies of Asymmetric Pitch/Plunge Flapping-The Secret of Biological flyers, AIAA paper 2001-0859, (2001).
Corke, T., Koga, D., Drubka, R. and Nabib, H., A New Technique for Introducing Controlled Sheets of Smoke Streaklines in Wind Tunnels, Proceedings of International Congress on Instrumentation in Aerospace Simulation Facilities, (1974), 74-80.
Dickinson, M. H. and Gotz, K. D., Unsteady aerodynamic performance of model wings at low Reynolds number, Journal of Experimental Biology, 174 (1993), 45-64.
Fejtek, I. and Nehera, J., Experimental study of flapping wing lift and propulsion, Journal of Aeronautical, 84 (1980), 28-33.
Liu, H., Ellington, C. P., Kawachi, K., Van den berg, C. and Willmott, A. P., A computational fluid dynamic study of hawkmoth hovering, Journal of Experimental Biology, 201 (1998), 461-477.
Okamoto, M., Yasuda, K. and Azuma, A., Aerodynamic Characteristics of the Wings and Body of a Dragonfly, Journal of Experimental Biology, 199 (1996), 281-294.
Saharon, D. and Luttges, M. W., Visualization of Unsteady Separated Flow Produced by Mechanically Driven Dragonfly Wing Kinematics Model, AIAA Paper 88-0569, (1988).
Singh, B., Ramasamy, M., Chopra, I. and Leishman, J. G., Insect-based flapping wings for micro hovering air vehicle: experimental investigations, American helicopter society international specialists meeting, (2004).
Van den Berg, C. and Ellington, C. P., The three dimensional leading-edge vortex of a 'hovering' model hawkmoth, Phil. Trans. R. Soc. Land., 352 (1997), 329-340.
Willmott, A. P., Ellington, C. P. and Thomas, A. L. R., Flow visualization and unsteady aerodynamics in the flight of the hawkmoth, Manduca sexta, Phil. Trans. R. Soc. Land., 352 (1997), 303-316.

Author Profile

Song Hak Kim received his B.S. degree in aerospace engineering from Korea Aerospace University in 2005. He is currently a graduate student in the Department of Aerospace and Mechanical Engineering at Korea Aerospace University. His research interest is bio-fluid mechanics in the field of aerospace engineering.

Jo Won Chang received his B.S. degree in aerospace engineering from the Korea Air Force Academy in 1982, and his M.S. and Ph.D. degrees from Seoul National University and KAIST in 1986 and 1999, respectively. He is currently an associate professor in the Department of Aeronautical Science and Flight Operation at Korea Aerospace University in Korea. His research interests include unsteady aerodynamics, bio-fluid mechanics, wind tunnel experiments, and flight tests.

Myong Hwan Sohn received his B.S. degree in aerospace engineering from the Korea Air Force Academy in 1977, and his M.S. and PhD degrees from Seoul National University and Georgia Institute of Technology in 1980 and 1986, respectively. He is currently a professor in the Department of Aerospace Engineering at the Korea Air Force Academy. His research interests include unsteady aerodynamics, bio-fluid mechanics, and flow control.